A Progressive Scan CCD Image Sensor for DSC Applications

Tetsuo Yamada, *Member, IEEE*, Katsumi Ikeda, Yong-Gwan Kim, Hideki Wakoh, Tetsuo Toma, Tomohiro Sakamoto, Kazuaki Ogawa, Eiichi Okamoto, Kazuyuki Masukane, Kazuya Oda, and Masafumi Inuiya

Abstract—A progressive-scan CCD image sensor with a standard double-layer poly-silicon is designed on a new architecture of pixel interleaved array named PIACCD. The pixel layout is estimated to enlarge the saturation voltage by 1.3 times and heighten the sensitivity with the 1.4 times enlarged equilateral aperture opened above each photodiode. The three-dimensional simulation ensures that the unique electrode pattern layout has an advantage to accelerate the signal charge transfer. The pixel interleaved array heightens the resolution by $2^{1/2}$ times in comparison with that of the same pixel number ITCCD in horizontal and vertical directions. The resolution characteristics fit to the fine pattern sensitivity of the human eye and the power spectrum distributions of nature scenes. The fabricated sensor, which has 2.4M pixels with 4.52 μm^2 pixel size, has provided the 1.3 times sensitivity and the dynamic range of 71 dB. The reproduced image has verified the resolution of PIACCD 1.4 times higher than that of the same pixel number ITCCD.

Fig. 1. Pixel size versus pixel number.

I. INTRODUCTION

MOST OF RECENT digital still cameras (DSCs) have over-1M-pixel CCD image sensor [1] to take high-resolution pictures, and they have been requested to have more pixel number to make the pictures high quality comparable with that taken by conventional film cameras. Generally, the pixel number should be increased without enlarging the imaging size, i.e. the chip size, to keep the sensor cost low and the optical lens system compatibility. Fig. 1 shows pixel size versus pixel number for widely used imaging sizes of consumer DSCs.

As shown, pixel size is reduced in inverse proportion to increase of pixel number. In case of half-inch imaging size, the 5.6 μm^2 size of 1M pixels is reduced to about 3.2 μm^2 by increasing the pixel number to 3M, which is 0.3 times pixel size reduction. The pixel size reduction lowers the sensitivity and narrows the dynamic range by the same reduction factor of 0.3 because they are roughly proportional to pixel size. The sensitivity and the dynamic range are main factors to determine the image sensor performance as well as the resolution. So conventionally, the high resolution is incompatible with the high sensitivity and wide dynamic range.

In DSC applications, two types of interline transfer CCD (ITCCD) image sensor have been mainly used. One is a progressive-s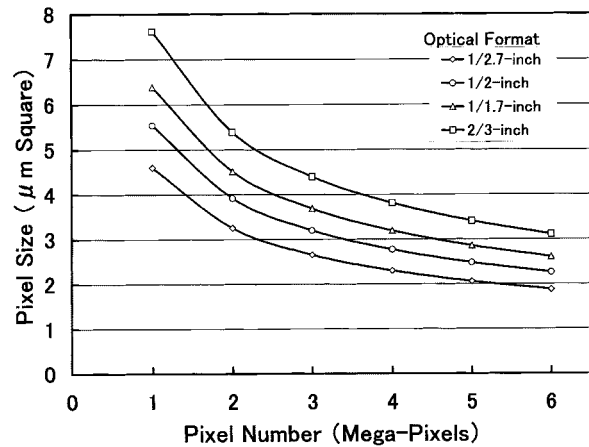can type, where vertical transfer CCD (VCCD) is constructed with three-layer polycrystalline silicon (poly-silicon) electrodes [2] or single-layer poly-silicon electrodes [3]. Those require an extra and sophisticated fabrication process.

Moreover, large area on the imaging region is occupied by extra electrode wiring between VCCDs, and this region acts as dead space in the silicon bulk. Another ITCCD is the interlace-scan type, which enables fabrication with a standard double-layer poly-silicon technology. Though it has the advantage of greater VCCD charge transfer, it essentially requires a precise mechanical shutter for DSC application. Furthermore, storage electrons in a photodiode are thermally emitted to an antiblooming drain after closing of the mechanical shutter [4]. It results in a severe loss of the maximum signal voltage (the saturation voltage). In this point of view, if a progressive scan CCD can be constructed with a standard double poly-silicon electrodes, it will offer the best solution for DSC applications.

The CCD image sensor presented here is developed to offer the best solution. That is to say, a progressive scan image sensor implemented in standard double-layer poly-silicon CCD is designed on the pixel interleaved array (PIA) CCD architecture for DSC applications. It arranges the pixels spatial phase alternation by line. The new sensor also solves the problem of incompatibility between high resolution and each of high sensitivity and wide dynamic range.

This paper is organized as follows. In Section II, the design concept and the pixel architecture are presented. Section III estimates the spatial efficiency in the unit pixel, which affects the dynamic range and the sensitivity, and confirms the charge transfer process, and discusses the resolution characteristics. Section IV introduces the synthetic composition of fabricated
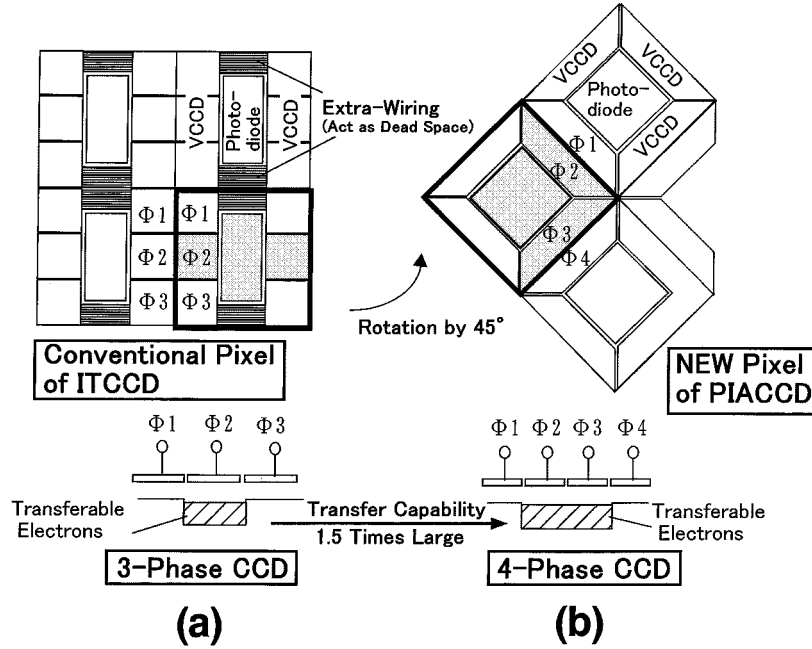
Fig. 2. Design concept of PIACCD.

sensor and the operations for DSC applications. The measurement results are given in Section V, and the work is summarized in Section VI.

II. DESIGN CONCEPT AND PIXEL ARCHITECTURE

A. Design Concept

At first, we will consider how to realize the progressive scan CCD image sensor with using a standard double-layer poly-silicon technology. For this purpose, we will study some of disadvantages of a conventional interline transfer CCD (ITCCD).

Fig. 2(a) shows the pixels of an ITCCD. The square region indicated by the bold line is a unit pixel. In this unit pixel, the photodiode is centered and the VCCD is on either side of the photodiode. As shown, both VCCDs are separated by the photodiode. So, extra wiring is required to supply the clock pulses to the every VCCD electrodes. As previously mentioned, the extra wiring region acts as dead space in the silicon bulk.

To minimize the extra wiring, a three-phase CCD fabricated with three-layer poly-silicon technology has been used in conventional.

The detailed structure is shown in Fig. 3(a). Approximately, the charge transfer capability of n-phase CCD [5] is given as

$$Q_T = Q_0 S_{CD}(n-2)/n \qquad (1)$$

where

Q_T maximum transferable charge;
Q_0 maximum storage charge density;
S_{CD} unit stage area of CCD.

For the three-phase CCD ($n = 3$), $Q_T = Q_0 S_{CD}/3$ is obtained from (1).

This means that only one electrode can store the signal charge, because two electrodes should form potential barriers in CCD channel, as shown in Fig. 2(c).

In case that a four-phase CCD ($n = 4$) replaces it, Q_T becomes $Q_0 S_{CD}/2$, which is 1.5 times larger than that of the three-phase CCD, as shown in Fig. 2(d). However, the four extra wiring lines on a plane occupy a larger area [3]. So, there is little difference of the total area loss between the three-phase and the four-phase type.

From this discussion, it can be concluded that the most important structural disadvantage of a conventional pixel is in the requirement of the extra wiring. In other words, the extra-wireless four-phase progressive scan VCCD is the best architecture to be developed. In order to remove the extra wiring, the same phase electrodes on both sides of the photodiode should be connected directly each other. It is impossible in conventional pixels.

To achieve this target, we rotate the pixel by 45°, as shown in Fig. 2(b), which is the concept of PIACCD. The central region in the unit pixel is the photodiode. VCCDs surround the photodiode and border on each other. So, this concept of pixel layout enables the use of a four-phase progressive scan VCCD without the area loss, and arranges the pixels' spatial phase alternation by line.

B. Pixel Architecture

Fig. 3 shows the actual layout of PIACCD in comparison with that of a conventional three-layer poly-silicon ITCCD. The pixels are filled closely in a zigzag with 3.2 μm pitch horizontally and vertically. The unit pixel is diamond shaped and is $3.2*2^{1/2}$ μm × $3.2*2^{1/2}$ μm (about 4.52 μm^2). This new and unique pattern layout is the key point of this work. The octagonal regions are photodiodes. The gray octagonal area is an aperture opened above each photodiode. As shown, the four-phase VCCDs are composed of standard double-layer poly-Si electrodes of $\Phi1$, $\Phi2$, $\Phi3$, and $\Phi4$. Each VCCD channel meanders along the photodiodes, and borders on the next VCCD channel without the extra wiring. In this way, PIACCD achieves the extra-wireless four-phase VCCD. By removing the extra wiring and using the
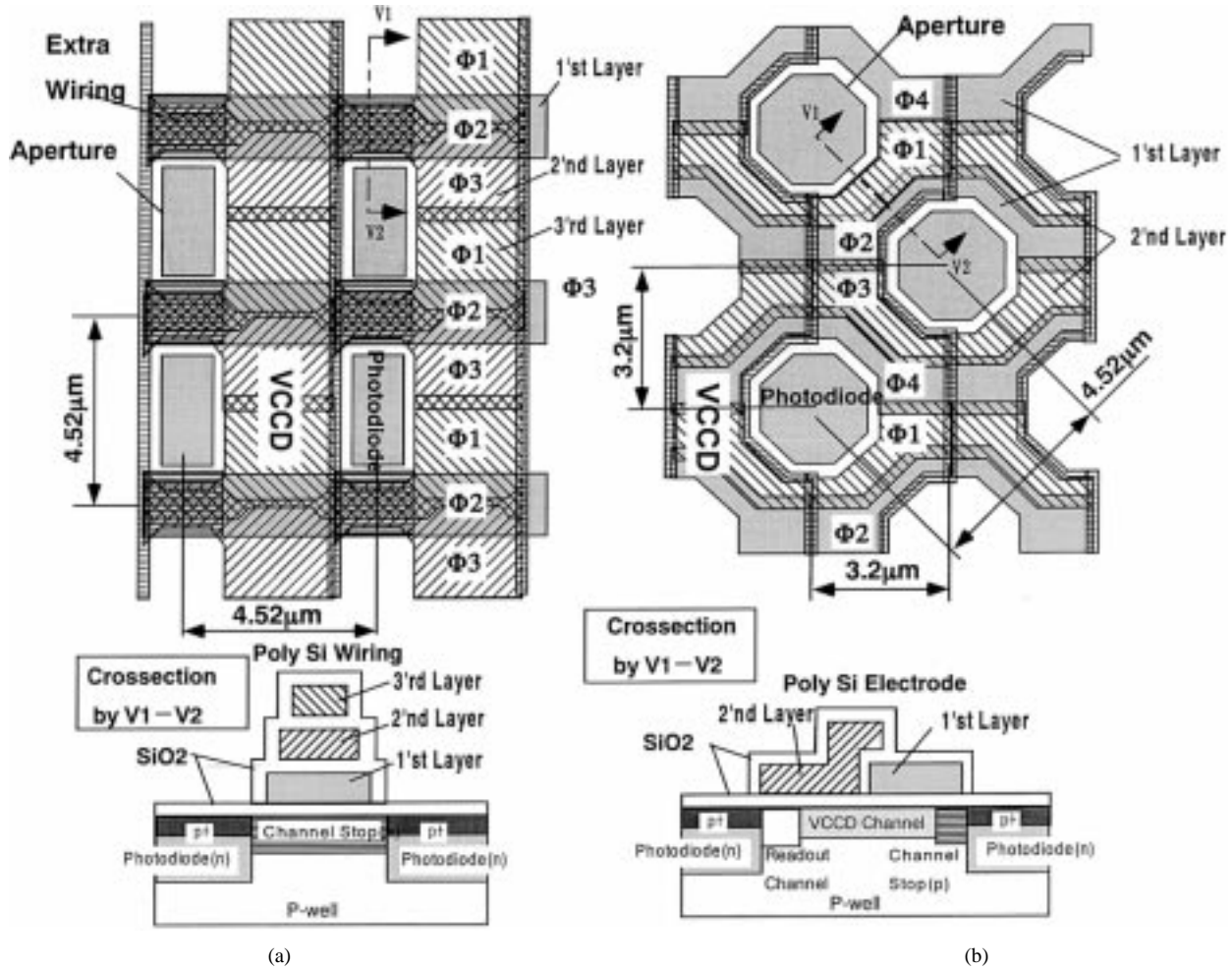
Fig. 3.   Pixel pattern layout. (a) ITCCD. (b) PIACCD.

four-phase VCCD, the active area of the photodiode and VCCD can be enlarged. Moreover, the enlarged equilateral aperture has an advantage to gather more rays of light passing through on-chip microlens than the ITCCD oblong aperture.

A cross section of the extra wiring area is shown at the bottom of Fig. 3(a). The three-layer poly-silicon lines form a high bump and cast a shadow on the photodiode with the rays of light angled by on-chip microlens. In case of PIACCD, the single-layer electrode either first layer or second layer surrounds almost peripheral of the photodiode as shown in Fig. 3(b), and hardly makes the shadow on the photodiode, which results in high sensitivity with the enlarged equilateral aperture. This pixel-interleaved arrangement achieves a higher resolution which will be described later.

III. DESIGN CONSIDERATION

A. Active Area Estimation

The active area S_{AC} means the total of photodiode area S_{PD} and charge storage area S_{ST} in VCCD, as shown in Fig. 4(b), and is given with (1) as

$$
\begin{aligned}
S_{AC} &= S_{PD} + S_{ST} \\
&= (\alpha + 1)S_{ST} \\
&= (\alpha + 1)(n - 2)/nS_{CD}
\end{aligned} \tag{2}
$$

where α is S_{PD} to S_{ST} ratio. S_{CD} is given as

$$
\begin{aligned}
S_{CD} &= S_{PX} - S_{CS} - S_{PD} \\
&= S_{PX} - S_{CS} - \alpha(n - 2)/nS_{CD} \\
&= (S_{PX} - S_{CS})/(1 + \alpha(n - 2)/n)
\end{aligned} \tag{3}
$$

where S_{PX} is the unit pixel area, and S_{CS} is the inactive area of the channel stop and transfer gate which controls the signal charge flow from the photodiode to the VCCD. In case of the PIACCD, S_{PX} is $2p^2$ for the pixel pitch p, and n equals 4. On the other hand, S_{CD} and S_{CS} can be squared geometrically as follows:

$$
S_{CD} = 2[2^{1/2}p - (2^{1/2} - 1)(c + w)]w \tag{4}
$$

$$
\begin{aligned}
S_{CS} = 2[2*2^{1/2}p - (5*2^{1/2}/2 - 2)w - (3*2^{1/2} - 9/4)c]c \\
\text{(for PIACCD)} \tag{5}
\end{aligned}
$$

where w is the VCCD channel width, and c is a common dimension of the channel stop width and the transfer length.

From (3)–(5), w is solved as a function of p, c, and α as

$$
w = w(p, c, \alpha). \tag{6}
$$

Their mathematical derivation is given in the Appendix. With substituting (4) and (6) into (2), S_{AC} is calculated as a function of p, c and α.
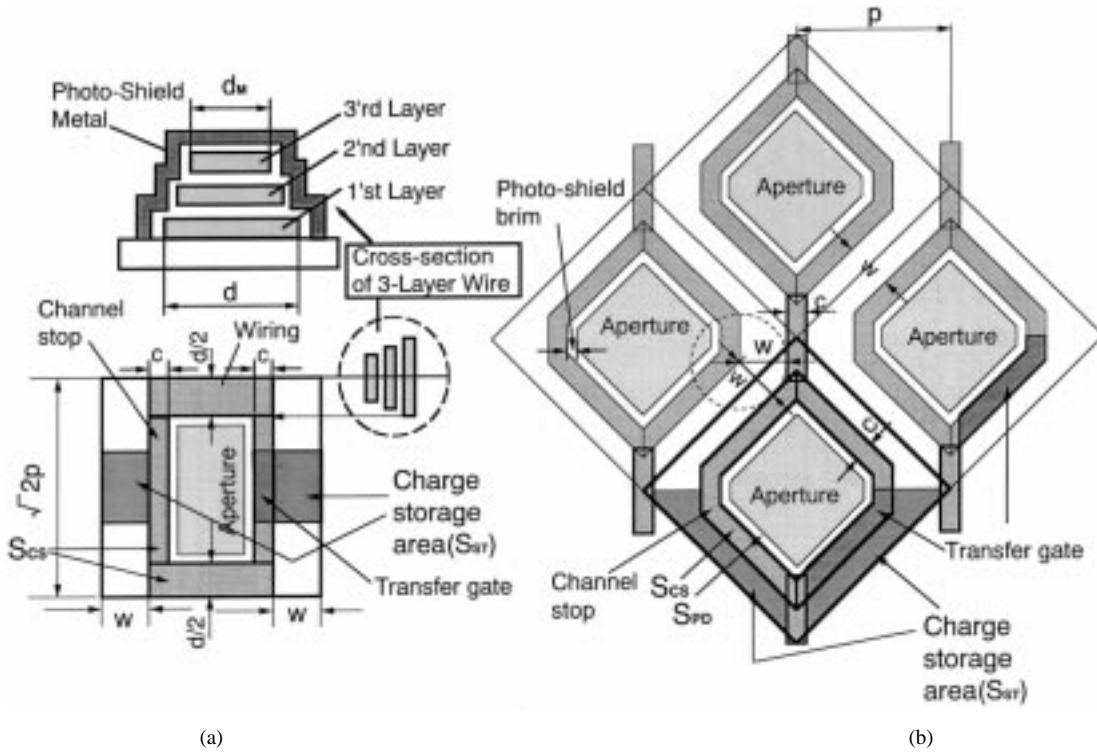
Fig. 4. Active area in the pixel. (a) ITCCD. (b) PIACCD.

In case of the same pixel size ITCCD, the horizontal and vertical pixel pitch is $2^{1/2}p$, $n = 3$, and S_{CS} additionally contains the extra wiring area, as shown in Fig. 4(a). S_{CD} and S_{CS} of ITCCD are also squared geometrically as

$$S_{CD} = 2^{1/2}pw \qquad (7)$$
$$S_{CS} = 2*2^{1/2}pc + (2^{1/2}p - w - 2c)d \qquad \text{(for ITCCD)} \qquad (8)$$

where d is the extra wiring width. Under this condition, w is derived from (3), (7) and (8) as

$$w = [2p^2 - (2*2^{1/2}c + 2^{1/2}d)p + 2cd]/[2^{1/2}(1 + \alpha/3)p - d] \qquad (9)$$

The active area S_{AC} of ITCCD can be also described as a function of p, c, d, and α by substituting (7) and (9) into (2).

For minimizing the area loss, c is given as the minimum dimension of the design rule. S_{PD} to S_{ST} ratio α is a optimizing parameter to keep the VCCD capacity a little larger than that of photodiode. For three-layer poly-silicon wire of ITCCD, the top wire has the minimum width d_M without dumping the gate control pulses, and the bottom wire is wider than the top wire to taper the side wall of the overlapped wires for ensuring the step coverage of photo-shield metal as shown in Fig. 4(a). So, d is defined as the bottom wire width.

For the present case of $c = 0.3$ μm, $\alpha = 1.6$ and $d = 1.0$ μm ($d_M = 0.6$ μm), the curves in Fig. 5 is calculated for the pixel pitch p, which shows relative active areas versus pixel size and are normalized by the active area of 4.6 μm^2 PIACCD pixel as $S_{AC}(p)/S_{AC}(p = 4.6/2^{1/2})$. Upper curve is PIACCD and lower is ITCCD. For 4.52 μm^2 pixel ($p = 3.2$ μm) of this case, the active area of PIACCD is about 1.3 times as large as that
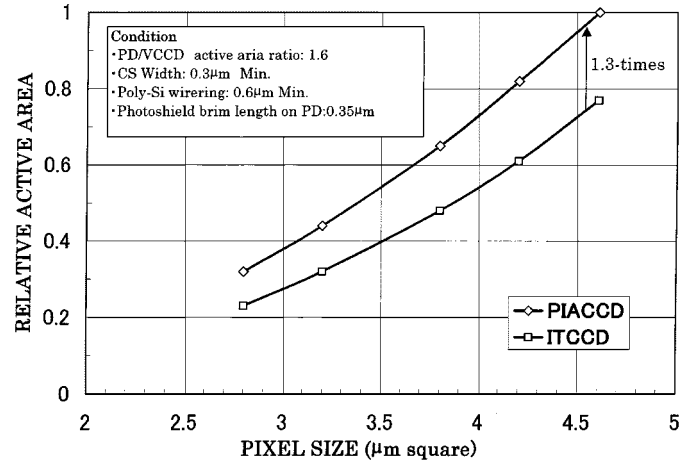

Fig. 5. Relative active area for pixel size.

of ITCCD. As the saturation voltage V_{SAT} of the image sensor is roughly proportional to this active area, without considering the depletion region formed by the reverse biased p-n junction between VCCD and channel stop, we can estimate V_{SAT} of PIACCD is about 1.3 times as large as that of ITCCD. Dynamic range is defined by V_{SAT} and dark noise level V_{DN} as $20 \log(V_{SAT}/V_{DN})$. So, that of PIACCD is widened by about 1.3 times with same noise level. The aperture size on the 1.3 times enlarged photodiode is expanded by 1.4 times with constant photo-shield brim length. The high spatial efficiency also means that PIACCD is suitable for finer pixel integration.

B. Charge Transfer in PIACCD

Fig. 6(a) shows the unique shaped four-phase electrodes of $\Phi1$, $\Phi2$, $\Phi3$, and $\Phi4$ in unit transfer stage of PIACCD. As the
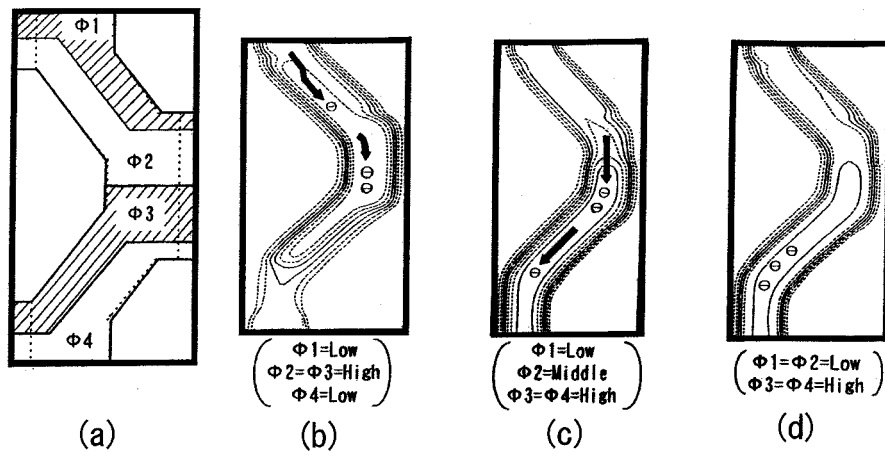
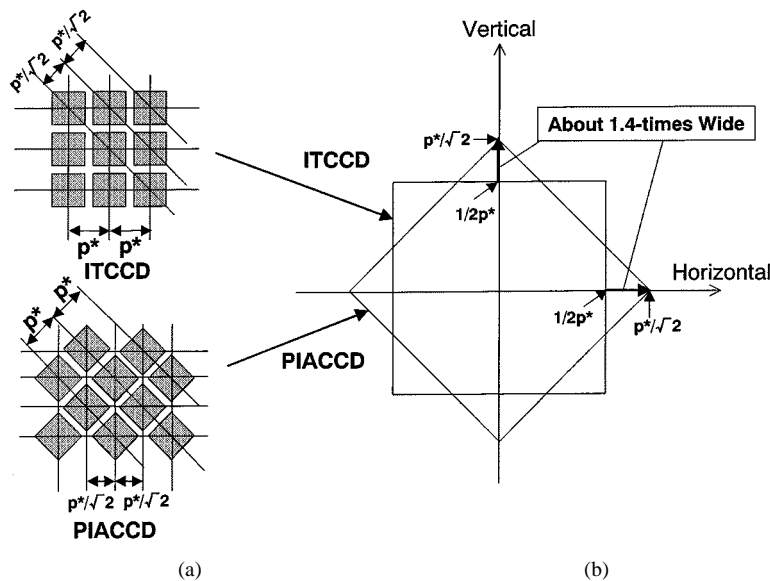Fig. 6.   Channel potential profiles in PIACCD.

Fig. 7.   (a) Pixel arrangement. (b) Nyquist limits of ITCCD and PIACCD.

unit transfer stage is twice as long as that of ITCCD, it is important to confirm whether PIACCD could transfer the signal electrons smoothly or not. Fig. 6(b) presents the channel potential contours under the condition that $\Phi2$ and $\Phi3$ are high level of 0 V, and $\Phi1$ and $\Phi4$ are low level of -8 V. This potential profile is calculated from the three-dimensional device simulator [6]. The electrons in the channel beneath $\Phi2$ and $\Phi3$ have been transferred from $\Phi1$ through the $\Phi1$–$\Phi2$ interface. This interface paralleled roughly to the charge transfer direction shortens the effective transfer length L_{eff}, and shortens the charge transfer time τ, because τ is roughly given by the relation of

$$\tau \sim L_{\text{eff}}^2 \quad [7].$$

Under the condition that $\Phi4$ becomes high and $\Phi2$ is falling toward low, the potential profile is changed as shown in Fig. 6(c), and the electrons flow toward $\Phi3$ and $\Phi4$. Under this transfer process, the electric field from the narrow electrode portion toward the wide electrode portion, which is generated by narrow channel effect, accelerates the charge transfer in this VCCD channel [8]. The potential profile under the condition

that $\Phi1$ and $\Phi2$ are high level, and $\Phi3$ and $\Phi4$ are high level is shown in Fig. 6(d). Under this condition, all electrons are stored beneath $\Phi3$ and $\Phi4$. The potential profile behavior through this process means that these unique-shaped electrodes of PIACCD can transfer the large number of signal electrons smoothly without sacrificing transfer speed.

C. Resolution Characteristics

Next the resolution characteristics of PIACCD are discussed and compared to that of ITCCD. Fig. 7(a) shows the pixel arrangement of ITCCD and PIACCD. The horizontal and vertical pixel pitch in ITCCD each is p^*, and that of PIACCD is p which equals $p^*/2^{1/2}$. These pixel pitches mean the horizontal and vertical spatial sampling pitches of images. So, Nyquist limits of ITCCD and PIACCD are given as $1/(2p^*)$ and $1/(2^{1/2}p^*)$, respectively, in the horizontal and the vertical axes, as shown in Fig. 7(b). It means that PIACCD widens the spatially frequency response, namely heightens the resolution, by $2^{1/2}$ in the horizontal and the vertical directions.

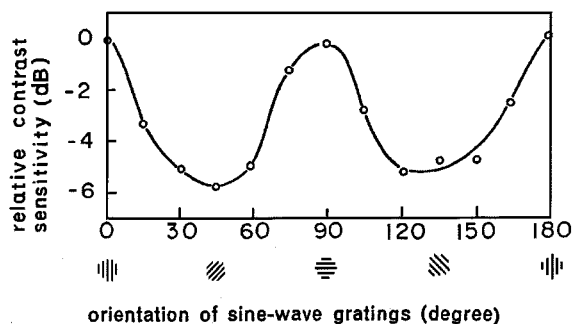However, in the 45° tilted directions, this resolution supremacy moves to ITCCD. Next, we will consider which

Fig. 8. Spatial response of the human visual system. (Data from Watanabe, *et al.*, 1968 [9])

Fig. 10. Concept of pixel interpolation for reproducing images.

Fig. 9. Average spatial power spectrum distribution of about 500 scenes.
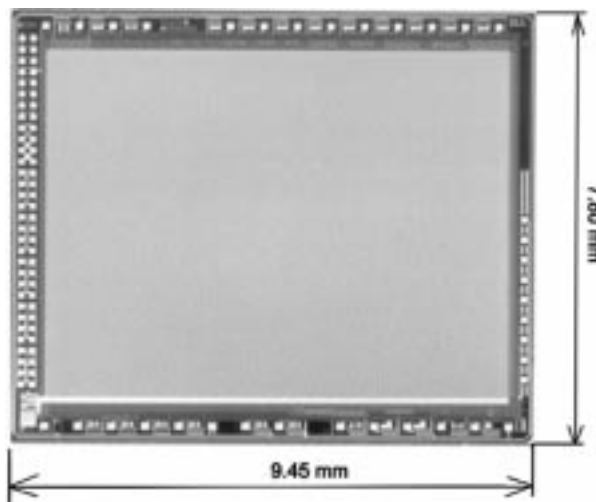
Fig. 11. Chip micrograph of the fabricated 2.4 Mpixel PIACCD.

resolution characteristics is suitable for DSC applications, ITCCD or PIACCD.

Fig. 8 shows relative contrast sensitivity of human visual system versus orientation of sine-wave gratings [9]. In this figure, zero (or 180)° means the vertical gratings, and 90° means the horizontal gratings. This curve shows that the human eye is most sensitive for the vertical and horizontal gratings, namely it has the highest resolution in vertical and horizontal directions. These resolution characteristics meet that of PIACCD.

Fig. 9 shows the average spatial power spectrum distribution of about 500 various scenes such as persons, animals, pastoral landscapes, city landscapes, and everything [10]. As shown, the high-frequency power spectrums concentrate in the vertical and horizontal directions. This spectrum distribution fits the Nyquist limit of PIACCD. As a result, from both properties of the human eye and natural-scenery points of view, the spatially interleaved pixels of PIACCD has optimized resolution characteristics for DSC applications.

Fig. 10 shows the final pixel arrangement of PIACCD to reproduce a scene picture. The spatially interleaved pixels can easily make the same number of virtual pixels in between the real pixels by a signal processing of pixel interpolation as shown [11].

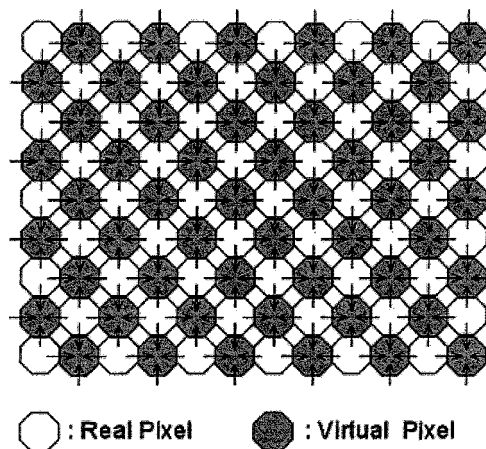As a result, the effective pixel number is increased by twice.

IV. FABRICATION AND OPERATION

Fig. 11 shows the actual fabricated PIACCD chip. It uses a standard double-poly Si technology. Chip size is 9.45 mm by 7.8 mm. A block diagram of this sensor is presented in Fig. 12. About 2.4M pixels are integrated zigzag with 3.2 μm pitch. The imaging size is 7.94 mm(H) $\times$ 5.95 mm(V).

The pixels forms the spatially phase alternation by line, and has the vertical antiblooming drain structure [12]. As shown, each four-phase VCCD meanders along the photodiodes toward the horizontal transfer CCD, and has ten clock lines to enable not only full-frame readout but also various modes such as every second line addressing, every fourth line addressing, signal mixings among vertically adjacent lines, and eight-phase clock operation for high speed and the mixed double-size charge transfer. These operation modes are used for video monitoring, auto-focusing control, and auto-exposure control. The horizontal transfer CCD is clocked on 3.3-V swing, and outputs the signals at 16.36 MHz rate through output circuitry. An example of color filter arrangement is also shown in Fig. 12. Green filters G cover the pixels located on square lattice points. Red R and blue B filters alternatively cover the phase shifted pixels. A diamond-shaped microlens is formed on the top of each pixel.
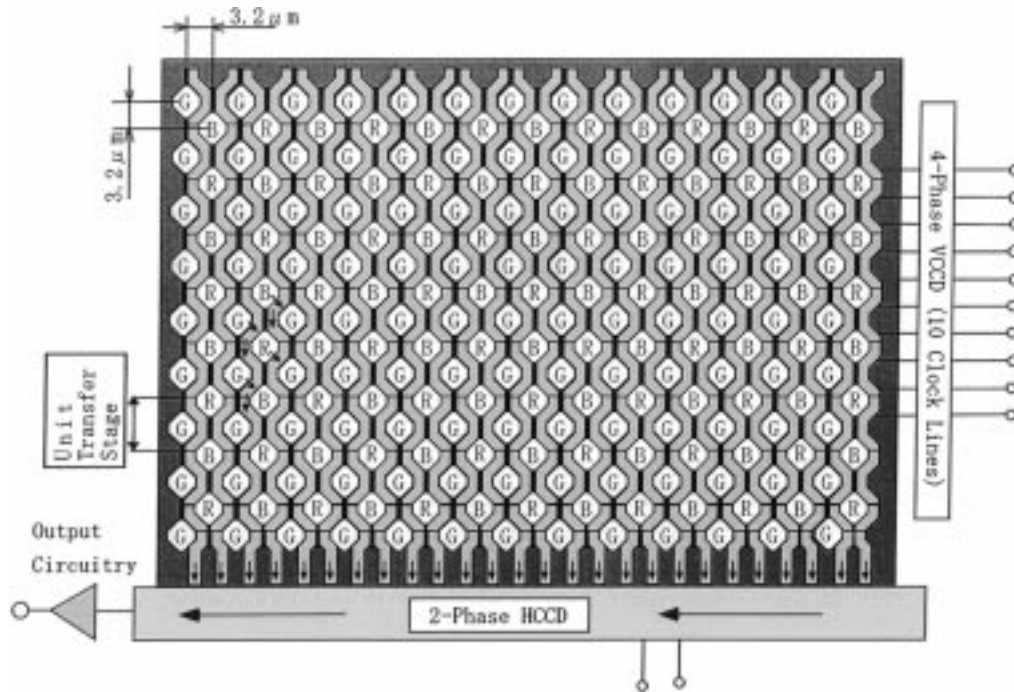
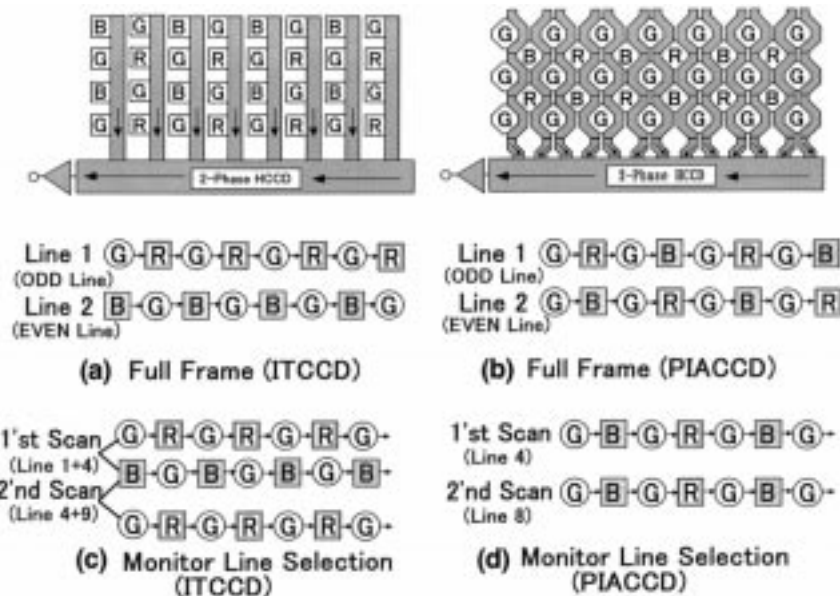Fig. 12.   Block diagram of the fabricated PIACCD.

Fig. 13.   Full-frame signal sequences: (a) ITCCD (Bayer). (b) PIACCD. Every fourth line selected signal sequences: (c) ITCCD (Bayer). (d) PIACCD.

In the case of full-frame readout, the VCCD is operated with four-phase clocks. The output signal sequence is shown in Fig. 13(b). Fig. 13(d) shows a signal sequence of the every fourth line addressing to make a real-time monitor on a electronic viewer such as a liquid crystal display in DSC. In this case, the VCCD is operated with eight-phase clocks to transfer signal electrons twice pixel distance in one clock period, and have charge transfer capacity three times larger than that of full-frame readout. So, it is easy to transfer the mixed double size electron packet. In the Bayer filter arrangement of ITCCD, each video line has merely two color signals of G and R or G and B as shown in Fig. 13(a) [3]. Therefore, two adjoining video lines are required to make one scanning line for a real-time video monitor as shown in Fig. 13(c), which needs to contain R, G, and B signals in every line, using a line memory. On the other hand, since each video line of PIACCD has three color signals of R, G, and B, a monitor scanning line can be easily made from any selected line without using a line memory.

V. EXPERIMENTAL RESULT

Fig. 14 shows the output voltage of PIACCD versus luminance for green-filter-covered pixel. Output voltage is measured
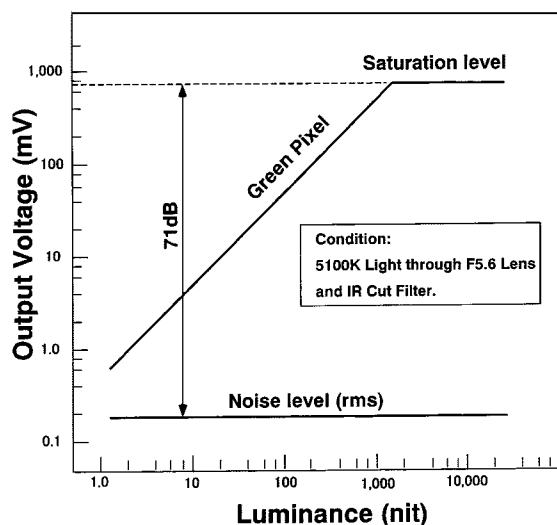
Fig. 14.   Photo-electric conversion characteristics of the fabricated PIACCD.

with our standard imaging condition under which the sensor is illuminated with the light coming through F5.6 lens and IR cut filter from 5100K color temperature source. For our standard luminance of 1200 nit and integration time of 1/60 s, the output of 340 mV is obtained. The saturation voltage is 700 mV, and the dark noise level measured after CDS is 0.19 mV$_{\text{rms}}$. So, the dynamic range from the noise level to the saturation level becomes 71 dB. The total charge transfer efficiency though VCCD and HCCD is over 99% (immeasurable level).
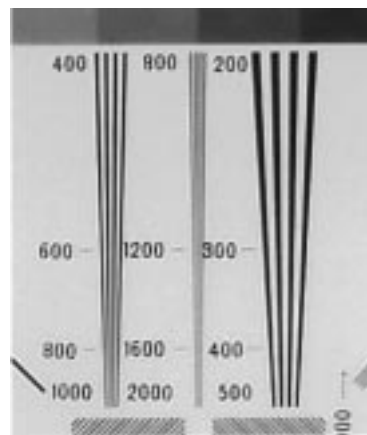
Fig. 15 shows a part of the reproduced resolution chart image. Fig. 15(a) is that taken by PIACCD, and Fig. 15(b) is that taken by a conventional ITCCD. Both image sensors have the same pixel number. Readable limitation of ITCCD is near 800-TV line and that of PIACCD is near 1100-TV line. This means that the resolution of PIACCD is about 1.4 times higher than that of ITCCD. Fig. 16 is an example of a full-frame natural scene taken by the fabricated sensor. Fig. 17(a) is a partly expanded picture in Fig. 16, and Fig. 17(b) is that taken by ITCCD. It is clear that PIACCD provides the higher quality.

The specification of new image sensor is summarized in Table I.

VI. CONCLUSION

New architecture of pixel interleaved array (PIA) CCD is presented in this paper. It is designed with the concept to maximize the space efficiency in a pixel pattern layout by rotating the pixel 45°. PIACCD has the advantages as follows:

1) A progressive scan CCD is realized using standard double-layer poly-Si technology.
2) The active area in a pixel is enlarged 1.3 times in comparison with the same pixel size ITCCD.
3) The 1.4 times enlarged equilateral shaped aperture opened above each photodiode has an advantage to heighten the sensitivity.
4) The resolution is fundamentally 1.4 times as high as that of ITCCD in horizontal and vertical directions. This prop-

(a)
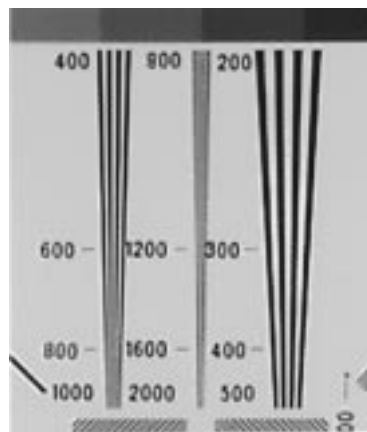
(b)

Fig. 15.   Part of reproduced image of the resolution chart taken by: (a) PIACCD. (b) ITCCD.

TABLE I
SPECIFICATIONS.

Device Structure	Progressive Scan PIACCD
Chip Size	9.45mm x 7.80 mm
Total Pixel Number	2.47M (2560(H) x 1930(V)/2)
Imaging Pixel Number	2.30M (2480(H) x 1860(V)/2) 4.60M (with Pixel Interpolation)
Pixel Spacing	4.52μm (Line Pitch : 3.2μm)
Imaging Area	7.94mm(H) x 5.95mm(V)
Color Filter	Green: Square Lattice Red & Blue: Mosaic
Saturation Voltage	700mV (25,000 electrons)
Sensitivity (Green)	340mV (5100K/IR cut,1200nit,F5.6)
Dynamic Range	71dB
Data Rate	16.36MHz (Clock Swing: 3.3V)

erty fits in both characteristics of human eye and natural scenery.

The 2.4M-pixel sensor with 4.52 μm pixel size has provided the sensitivity 1.3 times higher than that of conventional same pixel size ITCCD, and the dynamic range of 71 dB. 1100 TV-line pair could be read off in the reproduced resolution chart image. It corresponds to the 1.4 times high resolution.

Fig. 16.   Reproduced image of nature scene taken by PIACCD.

(a)   (b)

Fig. 17.   Part of the expanded image taken by: (a) PIACCD. (b) ITCCD.

APPENDIX
CALCULATION OF ACTIVE AREA IN PIACCD

First the VCCD in PIACCD pixel shown in Fig. 18 is squared. The VCCD area S_{CD} is decomposed into trapezoid area S_1 and parallelogram area S_2, and described as

$$S_{\mathrm{CD}} = 2(S_1 + 2S_2)$$

$$S_1 = (w+c)w, \quad S_2 = (p - w - c)w/2^{1/2}$$
$$S_{\mathrm{CD}} = 2[2^{1/2}p - (2^{1/2} - 1)(c+w)]w$$

where

p horizontal and vertical pixel pitch;
c common dimension of channel stop and transfer gate;
w VCCD channel width.
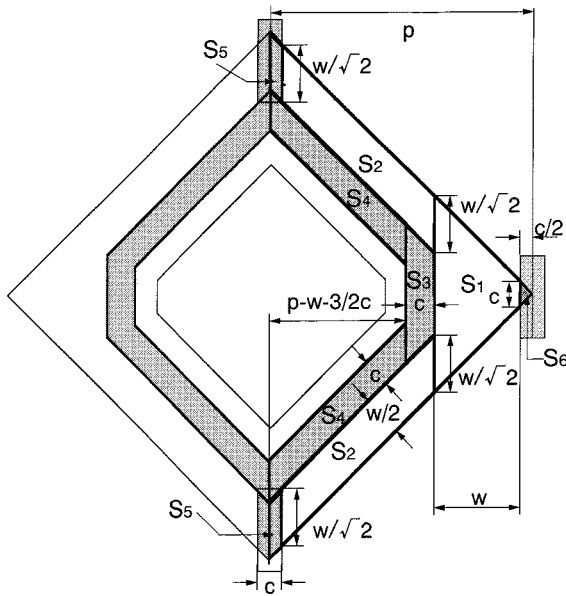
Fig. 18. Simplified pixel area in PIACCD.

Inactive area S_{CS} is also decomposed into trapezoid and parallelogram, and expressed as

$$S_{CS} = 2(S_3 + 2S_4 + 2S_5 + S_6)$$
$$S_3 = [(2 - 2^{1/2})w + 3c + (2 - 2^{1/2})w + c]c/2$$
$$= [(2 - 2^{1/2})w + 2c]c$$
$$S_4 = 2(p - w - 2/3c)$$
$$S_5 = cw/(2^*2^{1/2}), \quad S_6 = c^2/4$$
$$S_{CS} = 2[2^*2^{1/2}p - (5^*2^{1/2}/2 - 2)w$$
$$- (3^*2^{1/2} - 9/4)c]c.$$

In this case, four-phase VCCD ($n = 4$) is used. So, (3) becomes

$$S_{CD} = (2p^2 - S_{CS})/(1 + \alpha/2). \quad (10)$$

From (4) and (5), (10) is expressed as a quadratic function of w, and is solved for w as follows:

$$f_1(\alpha)w^2 + f_2(p, c, \alpha)w + f_3(p, c, \alpha) = 0$$

$$w(p, c, \alpha) = \{-f_2(p, c, \alpha) - [f_2(p, c, \alpha)^2 - 4f_1(\alpha)f_3$$
$$\cdot (p, c, \alpha)]^{1/2}\}/2f_1(\alpha) \quad (11)$$

$$f_1(\alpha) = (2^{1/2} -)(1 + \alpha/2)$$
$$f_2(p, c, \alpha) = -\{(1 + \alpha/2)2^{1/2}p - [7^*2^{1/2}/2 - 3$$
$$+ (2^{1/2} - 1)\alpha/2]c\}$$
$$f_3(p, c, \alpha) = p^2 - 2^*2^{1/2}cp + (3^*2^{1/2} - 9/4)c^2.$$

Substituting (4) and (11) into (2), S_{AC} is described as a function of p, c, and α.

REFERENCES

[1] T. Toma, A. Sakoda, A. Mikoshiba, K. Oda, R. Kawaguchi, and M. Inuiya, "A 2/3-inch 1.3M-pixel full-frame readout VT-CCD image sensor,", ITE Tech. Rep., vol. 18, Oct. 1994.

[2] T. Ishigami, A. Kobayashi, Y. Naito, A. Izumi, T. Hanagata, and K. Nakashima, "A 1/2-in 380k-pixel progressive scan CCD image sensor,", ITE Tech. Rep., vol. 17, Mar. 1993.

[3] M. Furumiya, K. Hatano, Y. Nakashiba, I. Murakami, T. Yamada, T. Nakano, Y. Kawakami, T. Kawasaki, and Y. Hokari, "A 1/2-inch 1.3M-pixel progressive-scan CCD image sensor employing 0.25 μm gap single-layer poly-Si electrodes," in ISSCC Dig. Tech. Papers, Feb. 1999, pp. 300–301.

[4] T. Yamada, H. Goto, H. Sekine, and N. Suzuki, "Image lag with photosensing element structure of CCD image sensor," in Proc. 1981 ITE Annu. Conv., July 1981, pp. 43–44.

[5] T. Yamada, K. Ikeda, and N. Suzuki, "A line-address CCD image sensor," in ISSCC Dig. Tech. Papers, Feb. 1987, pp. 106–107.

[6] H. Mutoh, "Simulation for 3-D optical and electrical analysis of CCD," IEEE Trans. Electron Dev., vol. 44, pp. 1604–1610, Oct. 1997.

[7] J. E. Carnes, W. F. Kosonocky, and E. G. Ramberg, "Free charge transfer in charge-coupld device," IEEE Trans. Electron Dev., vol. ED-19, pp. 798–808, June 1972.

[8] Y. D. Hagiwara, M. Abe, and C. Okada, "A 380H × 488 V CCD imager with narrow channel transfer gates," in Proc. 10th Conf. Solid-State Devices, vol. 18, Tokyo, Japan, 1978, JJAP Supplement 18-1, pp. 335–340.

[9] A. Watanabe, T. Mori, S. Nagata, and K. Hiwatashi, "Spatial sine-wave responses of the human visual system," Vision Res., vol. 8, pp. 1245–1263, 1968.

[10] M. Tamaru, M. Inuiya, T. Misawa, and T. Yamada, "Development of new structure CCD for digital still camera,", ITE Tech. Rep., vol. 23, 1999.

[11] H. Tamayama, O. Saito, and M. Inuiya, "High-definition still image processing system using a new structure CCD sensor," in IS&T/SPIE Symp. Electronic Imaging, Proc. SPIE, vol. 3965, Jan. 2000, pp. 431–436.

[12] Y. Ishihara, E. Oda, H. Tanigawa, N. Teranishi, E. Takeuchi, I. Akiyama, K. Arai, M. Nishimura, and T. Kamata, "Interline CCD image sensor with an antiblooming structure," in ISSCC Dig. Tech. Papers, Feb. 1982, pp. 168–169.

Tetsuo Yamada (M'79) was born in Shizuoka, Japan, on April 27, 1948. He received the B.S. and M.S. degrees in electrical engineering from Shizuoka University, Japan, in 1971 and 1973, respectively.

In 1973, he joined Toshiba Corporation, where he was engaged in development of CCD image sensors. In 1996, he joined Fujifilm Microdevices Company, Ltd., Miyagi, Japan, where he has continued his work on CCD image sensors for digital still camera applications. He is currently a CCD Design Manager.

Mr. Yamada received the National Grand Invention Awards graded as the Prize of the Minister of International Trade and Industry for the invention of the solid-state imager with vertical overflow drain, in 1990. He is a member of the IEEE Electron Devices Society and The Institute of Image Information and Television Engineers of Japan.

Katsumi Ikeda was born in Fukuoka, Japan, on December 30, 1964. He graduated from Nakatsu Technical High School, Oita, Japan, 1983.

He joined Toshiba Corporation in 1983, and Fujifilm Microdevice Company, Ltd., Miyagi, Japan, in 1999. He has been engaged in the research and development of solid-state image sensors.

Yong-Gwan Kim was born in Mokpo, Korea, on August 16, 1962. He received the B.S. degree from Inha University, Inchon, Korea, in 1984.

In 1987, he joined Goldstar Corporation, Korea. He was a Research Staff Member, and worked on development of CCD image sensors. Since 1997, he has been a Design and Development Engineer of mega-pixel CCD image sensors for digital still cameras with Fujifilm Microdevices Company, Ltd., Miyagi, Japan.

Hideki Wakoh was born in Miyagi, Japan, on July 27, 1973. He received the B.E. degree in materials science and engineering from Yamagata University, Yamagata, Japan, in 1996.

In 1998, he joined Fujifilm Microdevice Company, Ltd., Miyagi, Japan. Since then, he has been engaged in the research and development of solid-state image sensors.

Tetsuo Toma was born in Hokkaido, Japan, on December 13, 1951. He received the B.S. and M.S. degrees in chemistry from Hokkaido University in 1974 and 1976, respectively.

In 1976, he joined Fuji Photo Film Company, Ltd., Kanagawa, Japan, where he worked on the research and development of silver halide photosensitive emulsion, and solid-state imaging devices. Since 1991, he has been engaged in the development of solid-state imaging devices for digital still cameras with Fujifilm Microdevices Company, Ltd., Miyagi, Japan.

Mr. Toma is a member of the Japan Society of Applied Physics.

Tomohiro Sakamoto was born in Hokkaido, Japan, 1962. He received the B.E. degree from Tokai University in 1987.

He joined KSK Corporation, Tokyo, Japan, and worked on development of CCD image sensors. Since 1992, he has been engaged in research and development of megapixel CCD image sensors with Fujifilm Microdevices Company, Ltd., Miyagi, Japan.

Kazuaki Ogawa was born in Niigata, Japan, on April 27, 1951. He graduated from Takada technical high school, Niigata, in 1970.

He joined Sony Corporation in 1970 and Fujifilm Microdevices Company, Ltd., Miyagi, Japan, in 1990. He has been engaged in the research and development of solid-state image sensors.

Eiichi Okamoto received the B.S. degree in material science from University of Tokyo, Japan, in 1980.

He worked for Sanyo Electronics Corporation from 1980 to 1989. He was engaged in MOS device design of high-density static RAMs and dynamic RAMs. In 1990, he joined the Device Development Group, Fujifilm Microdevices Company, Ltd., Miyagi, Japan, and has been engaged in the research and development of solid-state image sensors.

Kazuyuki Masukane was born in Osaka, Japan, on August 31, 1946. He received the B. S. and M. S. degrees in physical chemistry from Osaka University in 1969 and 1971, respectively.

Since then, he has been with Fuji Photo Film Company, Ltd., Kanagawa, Japan, engaged in the research and development of the solid state image capturing systems for video still cameras, camcorders and digital still cameras. He is currently a Director of VLSI design with Fujifilm Microdevices Company, Ltd., Miyagi, Japan.

Kazuya Oda was born in Kanagawa, Japan, 1964. He graduated from the Nihon-kougakuin vocational school in 1984.

He joined Fuji Photo Film Company, Ltd., Kanagawa, Japan, in 1984. He is currently engaged in the research and development of CCD equipment of electronic still cameras.

Masafumi Inuiya was born in Kyoto, Japan, on April 14, 1946. He received the B.S. and M.S. degrees in applied physics from Osaka University, Osaka, Japan, in 1969 and 1971, respectively.

Since 1971, he has been with Fuji Photo Film Company, Ltd., Kanagawa, Japan, engaged in the research and development of solid-state image capturing systems for video still cameras, camcorders, and digital still cameras. He is currently a General Manager of electronic imaging product planning and development.

Mr. Inuiya is a member of The Institute of Image Information and Television Engineers of Japan.